Comparison of DCE-CT models for quantitative evaluation of Ktrans in larynx tumors

Article *in* Physics in Medicine & Biology · April 2015

DOI: 10.1088/0031-9155/60/9/3759

6 authors, including:

Jaap Oosterbroek
University Medical Center Utrecht
11 PUBLICATIONS **43** CITATIONS
SEE PROFILE

Edwin Bennink
University Medical Center Utrecht
49 PUBLICATIONS **628** CITATIONS
SEE PROFILE

Marielle E P Philippens
University Medical Center Utrecht
293 PUBLICATIONS **4,940** CITATIONS
SEE PROFILE

Cornelis P J Raaijmakers
University Medical Center Utrecht
169 PUBLICATIONS **3,442** CITATIONS
SEE PROFILE

Comparison of DCE-CT models for quantitative evaluation of K^{trans} in larynx tumors

J Oosterbroek, E Bennink, M E P Philippens, C P J Raaijmakers, M A Viergever, H W A M. de Jong

Division of Medical Imaging, University Medical Centre Utrecht

E-mail: J.Oosterbroek@umcutrecht.nl

Abstract

Dynamic contrast enhanced CT (DCE-CT) can be used to estimate blood perfusion and vessel permeability in tumors. Tumor induced angiogenesis is generally associated with disorganized microvasculature with increased permeability or leakage. Estimated vascular leakage (K^{trans}) values and their reliability greatly depend on the perfusion model used. To identify the preferred model for larynx tumor analysis, several perfusion models frequently used for estimating permeability were compared in this study. DCE-CT scans were acquired for 16 larynx cancer patients. Larynx tumors were delineated based on whole-mount histopathology after laryngectomy. DCE-CT data within these delineated volumes were analyzed using the Patlak and Logan plots, the Extended Tofts Model (ETM), the Adiabatic Approximation to the Tissue Homogeneity model (AATH) and a variant of AATH with fixed transit time (AATHFT). Akaike's Information Criterion (AIC) was used to identify the best fitting non-linear model e.g. the model with the lowest AIC. K^{trans} values from all models were compared with this best fitting model. Correlation strength was tested with two-tailed Spearman's rank correlation and further examined using Bland-Altman plots. AIC was lowest in 72% of all voxels for AATHFT, 18% for ETM and 10% for AATH. The overall median of individual patient medians K^{trans} estimates were 14.3, 15.1, 16.1, 2.6 and 22.5 mL/100g/min for AATH, AATHFT, ETM, Patlak and Logan respectively. K^{trans} estimates for all models except Patlak were strongly correlated ($p < 0.001$). Bland-Altman plots show large biases but no significant deviating trend for any model other than Patlak. AATHFT was found to be the preferred model among those tested for estimation of K^{trans} in larynx tumors.

1 Introduction

Tumor induced angiogenesis is generally associated with disorganized micro-vasculature with increased permeability or leakage. Using Dynamic Contrast-Enhanced Computed Tomography imaging (DCE-CT) properties of the microvascular system can be estimated in terms of perfusion parameters, including intravascular blood volume, blood flow and leakage (K^{trans}). Therefore DCE-CT can be used for tumor identification, delineation and characterization.

The most frequently used perfusion parameter for analyzing tumors is K^{trans}. In head and neck tumors, K^{trans} estimation using DCE-CT has been used to predict treatment outcome (Kim *et al* 2010, Chawla *et al* 2011), to identify hypoxic regions (Newbold *et al* 2009) and assess mandibular invasion (Van Cann *et al* 2008).

Analysis of DCE-CT data requires perfusion models that describe how tissue micro-vasculature alters the arterial contrast bolus, often referred to as the Arterial Input Function (AIF), into a locally measured Time Attenuation Curve (TAC). The relationship between AIF and TAC is usually described by a convolution with a third function; a so called Impulse Response Function (IRF). Most perfusion models describe the shape of this IRF and therefore play a crucial role in perfusion analysis since they form the bridge between raw image data and perfusion parameters.

Commonly used perfusion models used to estimate K^{trans} are the Adiabatic Approximation to the Tissue Homogeneity model (St. Lawrence and Lee 1998) (AATH), the Extended Tofts Model (Tofts *et al* 1999) (ETM) and the Patlak (Patlak *et al* 1983) linearization. A variant of at least one of these three models features in the majority of commercially available DCE-CT analysis software (Miles *et al* 2012). Because estimation the mean transit time parameter using AATH is often problematic, a version of AATH with Fixed mean Transit time (AATHFT) is included here.

Estimation of extravascular distribution volumes in head and neck tumors (Tawfik *et al* 2011, Bisdas *et al* 2007) indicate the presence of not only leakage, but also a substantial back-flow into the vessels. In contrast with AATH and ETM, which assume reversible leakage, Patlak assumes irreversible leakage (meaning no back-flow) of tracer to the Extravascular Extracellular Space (EES), which may invalidate it for use in tumor DCE-CT. Yet, Patlak is still often used for the estimation of K^{trans} in tumors (Miles *et al* 2012, Bisdas *et al* 2008, Kambadakone and Sahani 2009) and is therefore included in this research. The Logan plot (Logan *et al* 1990) is an alternative linearization that does model contrast agent back-flow and might therefore be an improvement over Patlak linearization for the estimation of K^{trans}.

Although earlier evaluations of AATH and ETM for perfusion analysis of other tumor types have been reported, to our knowledge no such systematic comparison of DCE-CT models in the head and neck region has been published. This study aims to compare AATH, AATHFT, ETM and the Patlak and Logan linearizations in terms of accuracy for estimating K^{trans} in larynx tumors.

2 Methods

AATH, AATHFT, ETM, Patlak and Logan can be used to estimate vascular permeability which is commonly quantified by estimating the rate of vascular leakage (K^{trans}). In addition, these models can also be used to estimate other perfusion parameters including blood flow (F), intravascular blood volume (V_i), mean intravascular transit time (T_i), reverse leakage rate (K_{ep}) and extravascular distribution volume (V_d). Table 1 shows an overview of the perfusion models and the parameter they can be used to estimate.

Table 1. Parameters estimated by the perfusion models. Plus symbols indicate the parameters estimated by the model.

Models	K^{trans}	K_{ep}	V_d	V_i	F	T_i
AATH	+	+	+	+	+	+
AATHFT	+	+	+	+	+	-
ETM	+	+	+	+	-	-
Patlak	+	-	-	+	-	-
Logan	+	+	+	-	-	-

2.1 Non-linear regression

Estimation of perfusion parameters using non-linear models such as AATH, AATHFT or ETM is done using non-linear regression (NLR). For this the TAC is a result of the convolution between the arterial input function AIF and the IRF:

$$TAC(t) = AIF(t) \otimes IRF(t) \quad \textbf{(1)}$$

In DCE-CT, the AIF can be measured from a large artery in the vicinity of the tumor and TAC can be measured in voxels within the tumor. Once the AIF and the TAC are known, we can reconstruct the best fitting IRF described by a perfusion models such as AATH, AATHFT or ETM. The perfusion parameters of AATH, AATHFT and ETM were estimated by minimizing the mean square error between the measured and computed TACs using a Nelder-Mead optimizer.

2.2 Delay

AATH, AATHFT and ETM include a delay parameter (T_d) that describes the time it takes for the bolus to travel from the AIF location to the location of the measured TAC. The Patlak and Logan linearizations cannot estimate delay on their own, yet delay can be incorporated by estimating delay by means of a non-linear model and then shifting the AIF or TAC accordingly. This would once again make NLR a requirement for the Patlak and Logan linearizations. This is undesirable due to the larger complexity and computation cost of NLR.

2.3 AATH and AATHFT

In the AATH model, all particles have the same transit time and leakage is reversible. The function for the IRF is given in equation 2. An example of a typical AATH IRF as found in tumor tissue is shown in figure 1.

$$IRF(t) = \begin{cases} 0 & t < T_d \\ F & T_d \le t < T_d + T_i \\ K^{trans} * e^{-(t-T_i-T_d)K_{ep}} & T_d + T_i \le t \end{cases} \begin{matrix} \text{delay} \\ \text{plug flow} \\ \text{leakage} \end{matrix} \quad \textbf{(2)}$$

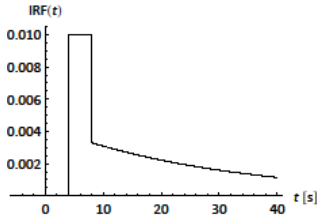

Figure 1. An example of a typical AATH IRF as found in tumor tissue.

Although in principle the transit time T_i is a free model parameter, in practice it is difficult to estimate. Increases in T_i and V_d both widen the first pass bolus of a TAC in a similar way, and their effects can

only be distinguished in DCE-CT time series with a high temporal resolution. But even when the protocol sampling frequency is theoretically sufficient and V_d is small, noise makes it difficult to get a reliable estimate of T_i (Kershaw and Cheng 2010). Therefore we included a variant of AATH with a fixed value for T_i. (AATHFT), as suggested in previous publications (Jeukens *et al* 2006, St. Lawrence and Lee 1998, Kershaw and Cheng 2010). Initial experiments showed that AATH with a fixed T_i value of 4 seconds produced the smallest mean squared errors averaged over all patients, and is therefore used in this study.

2.4 Extended Tofts

The permeability section in ETM is identical to that of AATH, however its perfusion section does not explicitly model tissue flow. Instead the arterial phase is modeled by adding the arterial concentration multiplied by the blood volume fraction to the tissue signal. In the IRF, this contribution is modeled with a Dirac-delta pulse multiplied by V_i (measured in volume faction). In contrast with AATH, which separates the V_i, T_i and F parameters, the ETM parameters are lumped into a single parameter V_i. From a different perspective, it could be interpreted as AATH with a fixed T_i value of 0 seconds. ETM is frequently used in tumor DCE-CT and DCE-MR processing (Korporaal *et al* 2010, Yang *et al* 2010, Sanz *et al* 2008, Korporaal *et al* 2012, Port *et al* 2010). The IRF for ETM is shown in equation 3. An example of the IRF can be found in figure 2.

$$IRF(t) = \begin{cases} 0 & t < T_d \\ \delta(t - T_d) * V_i + K^{trans} * e^{-(t-T_d)K_{ep}} & T_d \le t \end{cases} \begin{matrix} \} \text{ delay} \\ \} \text{ leakage} \end{matrix} \quad \textbf{(3)}$$

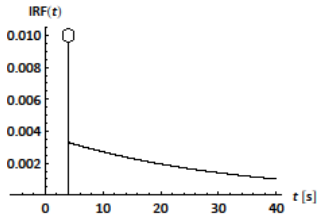

Figure 2. An example of a typical ETM IRF as found in tumor tissue.

2.5 Linearizations

Linearizations are models for estimating perfusion that are characterized by reducing tracer kinetic model into two-parameter, linear regression problems. Two well-known linearizations are the Patlak plot and the Logan plot. For linearization of the equations underlying the Patlak (equation 4) and Logan (equation 5) models are reformulated as linear equations with known x(t) and y(t), which can be displayed in a plot. Perfusion parameters can be estimated by linear least-squares fitting of the slope and intercept. Linearization generally provides a more robust fit and is computationally far less expensive than NLR. However linearizations lack the flexibility of NLR methods. Moreover not all models can be converted to a linear form.

$$\frac{TAC(t)}{AIF(t)} = K^{trans} \frac{\int_0^t AIF(\tau)d\tau}{AIF(t)} + V_i \quad \textbf{(4)}$$

$$\frac{\int_0^t TAC(\tau)d\tau}{TAC(t)} = V_d \frac{\int_0^t AIF(\tau)d\tau}{TAC(t)} - \frac{1}{K_{ep}} \quad \textbf{(5)}$$

Examples of an AIF and TAC are shown in figure 3, as well as the resulting Patlak and Logan plots. The linearizations discussed here require a stable state in which the tracer concentration in the vascular compartment and the EES reached a (near) equilibrium. The slope of the resulting line and the intercept with the y-axis or x-axis can be taken as estimates for various perfusion parameters. All data before the stable state are discarded. After inspection of the Patlak and Logan plots, we chose 60s as the first stable state point for all patients.

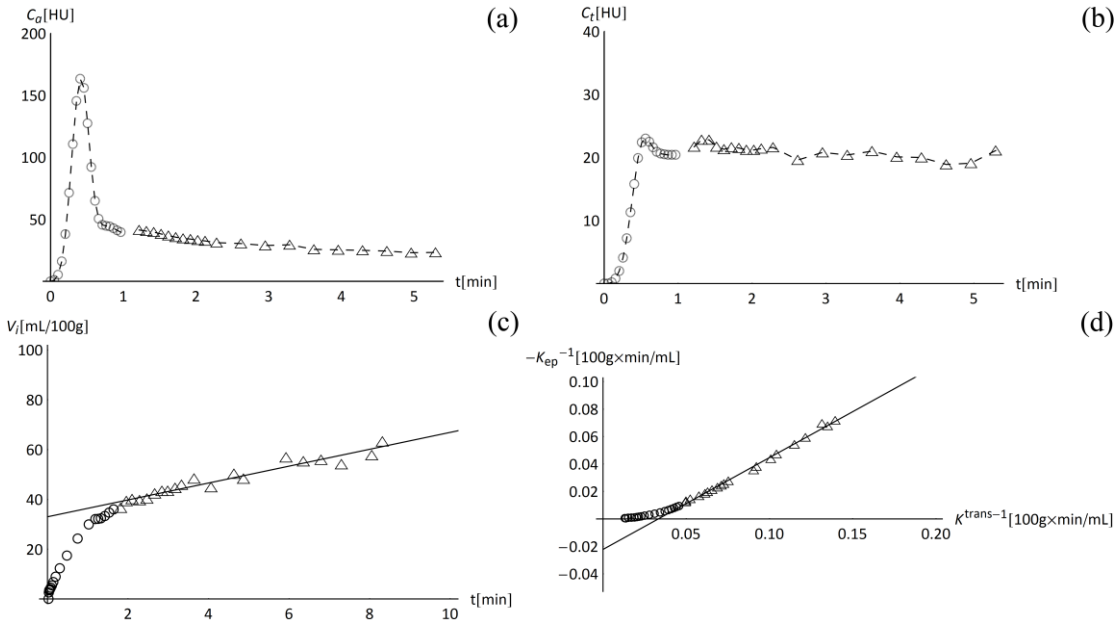

Figure 3. Example of the Patlak and Logan plot. (a) AIF, (b) TAC, (c) Patlak plot applied to the AIF and TAC of (a) & (b), (d) Logan plot applied to the AIF and TAC of (a) & (b). Circles are time points before 60s, triangles are time points after. The straight lines in (c) and (d) are least squared regressions after 60s. Patlak slope (K^{trans}) is 3.35 mL/100g/min and intercept (V_i) is 33.0 mL/100g. Logan slope is 0.67 (V_d), y-intercept (-1/K_{ep}) is -0.022 100g min/mL and x-intercept(1/K^{trans}) is 0.033 100g min/mL resulting in a K^{trans} of 30.3 mL/100g/min.

2.6 Patients

DCE-CT data were acquired for 16 patients with T3 or T4 squamous cell carcinoma within the laryngeal or hypopharyngeal area eligible for surgical resection. One patient was excluded because the image quality of the scans were compromised by severe motion. Another patient was excluded because a large biopsy was taken between the DCE-CT scan and the laryngectomy. The remaining 14 patients (mean age 60.5 +/- 7.8, 13 men and 1 woman) were included in this study, with primary T3 (n = 1) or T4 (n = 13) histologically proven squamous cell carcinoma of the larynx or hypopharynx. The study was approved by the medical ethics committee of the University Medical Centre Utrecht. After imaging, patients received a complete laryngectomy. Delineation of the tumor volume on histopathology and the subsequent translation of the delineations to the DCE-CT was described earlier by our group (Caldas-Magalhaes *et al* 2012).

2.7 Acquisition and Preprocessing

Patients were scanned fixated by their treatment masks. Coinciding with the start of the scans, 50 mL of iodine contrast (Iopromide, Ultravist, 300 mg/mL iodine, Bayer HealthCare Pharmaceuticals, Berlin, Germany) was injected into the cubital vein at a rate of 5 mL/s followed by a 40 mL saline flush at a rate of 5 mL/s by using a dual power injector. The scans were acquired using a Philips Brilliance iCT scanner (Philips Healthcare, Best, The Netherlands). The acquisition settings were 128 slices, 120 kVp, 200 mAs, 50mL iodine contrast agent (5 mL/s). The number of CT acquisitions was 20, 10 and 10, with intervals of 3, 6 and 20 s, respectively. The field-of-view of was approximately 180×180 mm2 with an axial coverage of 65-70 mm. The scans were reconstructed in a 512×512 matrix with 0.35x0.35x1.25 mm voxels without slice overlap (filtered backprojection, Philips B filter). After reconstruction, elastic registration was performed using the elastix toolbox (Klein *et al* 2010). The final preprocessing steps were the use of a temporal Gaussian filter (SD = 5s), followed by the bilateral TIPS filter with a spatial kernel size (SD) of 3mm, and a profile-similarity kernel size (SD) of 200 HU^2 (Mendrik *et al* 2011) to reduce noise. The first frame of the DCE series was considered free of contrast and was used as the background scan. The background scan was subtracted from all subsequent scans to create attenuation curve images. Only voxels with a background HU value in the range of -20 to 70 in this frame inside the tumor delineated on histology were included in the analysis. The AIFs were selected manually from the internal carotid artery. All estimates of V_i, F, K^{trans} and K_{ep} were corrected for changes in hematocrit inside small vessels (Konstas *et al* 2009).

2.8 Statistical analysis

Parameter maps were generated inside the tumor for visual inspection. Akaike's Information Criterion (AIC) (Akaike 1974) was used to determine the NLR-model (AATH, AATHFT and ETM) with the best fit between the models generated TACs and the measured TACs for every voxel separately. Because Patlak and Logan cannot be used to generate TACs they are not included in this analysis. AIC values were corrected for small sample sizes. The NLR-model with the lowest AIC value for the most voxels for the greatest number of patients was considered to have the best fit. Medians of patient medians and interquartile ranges of patient medians for the various parameters were calculated in order to compare estimates against values found in literature. The resemblance of the K^{trans} values between the various models was studied with a Spearman's ranked correlation test, which was considered significant at $p<0.01$. Models were compared against the model with the best fit using Bland-Altman plots of per patient median K^{trans} values to identify biases and trends.

3 Results

3.1 Model evaluation

The AATHFT model had the lowest AIC values for over 50% in all voxels for every patient (figure 4). The patient-weighted mean percentages (mean of means) of the lowest AIC were 10% for AATH, 72% for AATHFT and 18% for ETM. AATHFT had the first or second lowest AIC in 96% of all voxels of all patients.

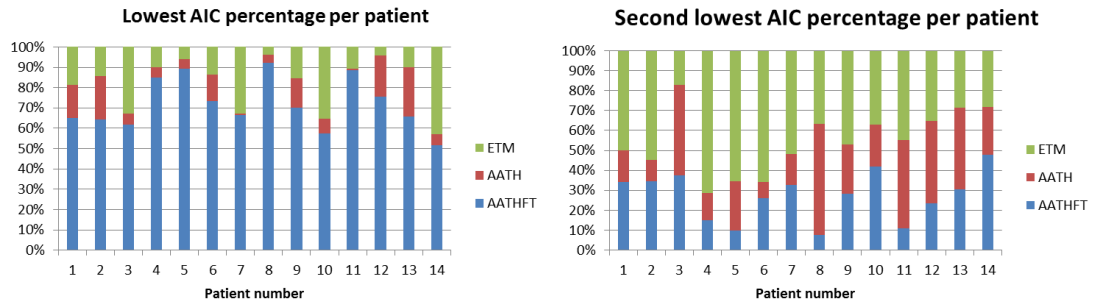

Figure 4. Results of the AIC analysis. For each patient the bar plot shows in what percentage of the voxels the AIC for a specific model was lowest (left) or second lowest (right).

3.2 Median values

All models except Patlak showed median parameter estimates with overlapping inter-quartile ranges (Table 2). Flow estimates for AATHFT were derived from V_i estimates using a fixed transit time of 4s. AATH, AATHFT and ETM showed increasing estimates of K^{trans} with decreasing estimates of V_i. The Logan model showed the highest estimates of K^{trans} but provided no estimates of V_i.

Table 2. Model parameters for the evaluated perfusion models. Perfusion parameter values shown are medians of patient medians. Below each value interquartile ranges of patient medians are shown.

	K^{trans} (mL/100g/ min)	K_{ep} (mL/100g/min)	V_d (a.u.)	V_i (mL/100g)	F (mL/100g/ min)	T_i (s)
AATH	14.3 (9.3 19.0)	31.8 (21.3 43.7)	0.46 (0.35 0.58)	6.2 (2.1 10.1)	32.3 (15.1 72.4)	6.8 (2.0 17.6)
AATHFT	16.1 (10.8 21.0)	34.8 (24.0 46.9)	0.47 (0.36 0.59)	5.2 (2.8 7.2)	77.8 (41.3 107.6)	
ETM	17.1 (11.2 23.0)	36.0 (24.6 47.9)	0.49 (0.38 0.63)	3.6 (0.0 5.9)		
Patlak	2.6 (1.5 3.7)			23.2 (9.6 32.1)		
Logan	22.5 (15.1 30.3)	42.3 (30.6 60.8)	0.51 (0.39 0.63)			

3.3 Parameter maps

Visual inspection of the parameter maps (figure 5) revealed a strong correlation between the models, especially for K^{trans}, K_{ep} and V_d. Patlak K^{trans} parameter maps showed no similarity to parameter maps computed using other models. High spatial noise was observed in the parameter maps generated by AATH and ETM.

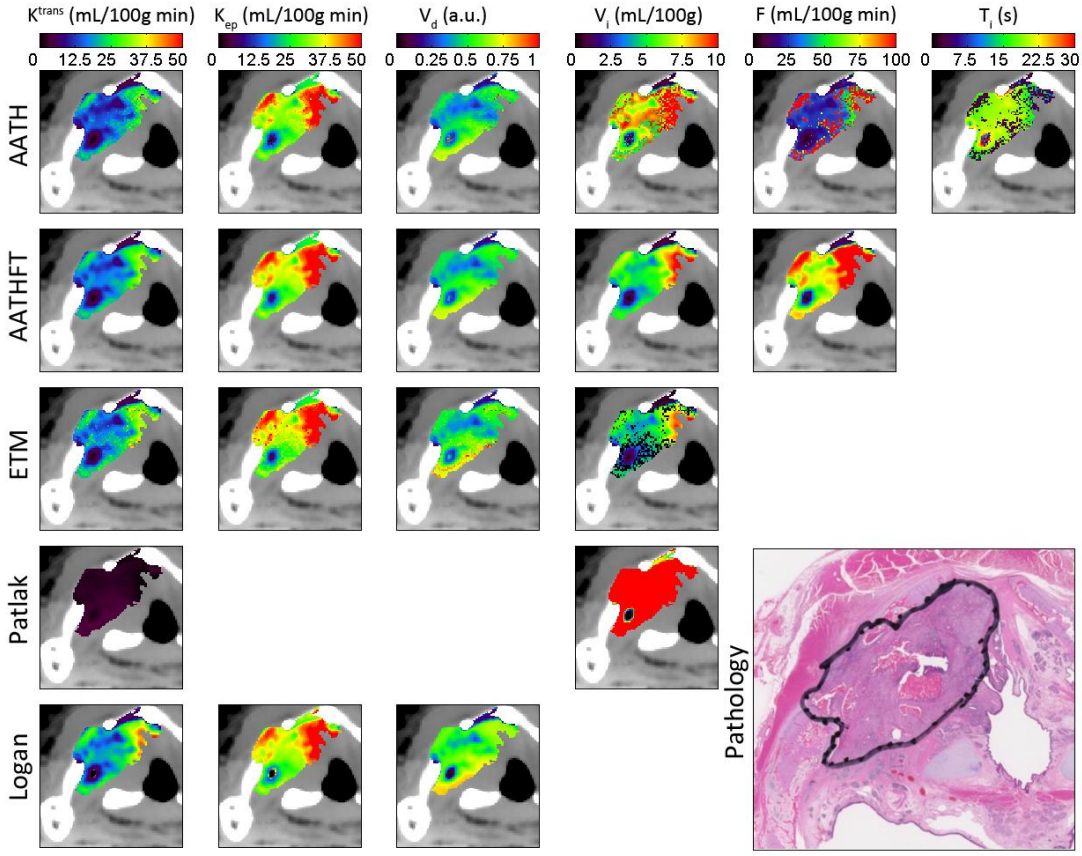

Figure 5. Parameter estimates within a larynx carcinoma represented as parameter maps. In the area outside the tumor the precontrast-CT values are shown for anatomical refence. Hematoxylin and eosin stained histological section is shown in the lower right corner. The black line is the delineation based on histopathology translated to the DCE-CT. Because the pathology slices are not completely aligned with the DCE-CT slices, the delinations do not match exactly.

3.4 Correlation of vascular leakage estimates.

Vascular leakage estimates for all models except Patlak showed strongly two-tailed significant correlation ($P < 0.001$) (Table 3).

Table 3. Correlation coefficients (Spearman's Rho and P values) of patient median Ktrans estimates for the five evaluated models.

	AATHFT	ETM	Patlak	Logan
AATH	0.94 P < 0.001	0.94 P < 0.001	0.36 P = 0.205	0.96 P < 0.001
AATHFT		0.98 P < 0.001	0.37 P = 0.188	0.94 P < 0.001
ETM			0.40 P = 0.153	0.91 P < 0.001
Patlak				0.26 P = 0.371

3.5 Bland-Altman plots of K^{trans}

Bland-Altman plots comparing AATHFT and other models for estimating K^{trans} (figure 6) showed significant biases for all models, with the strongest bias for Patlak and Logan. Variation within all models was in the order of their individual bias. The AATHFT-Patlak plot was the only one showing a strong trend between the mean of the AATHFT patient median and Patlak patient median value and the difference between the two.

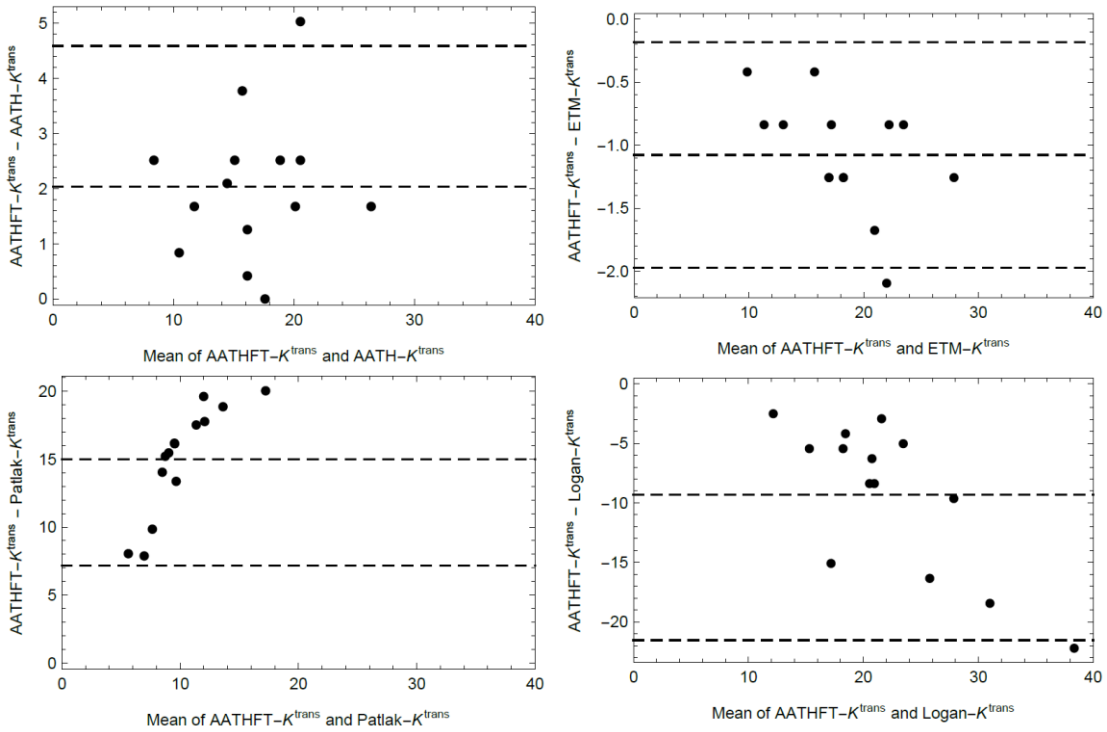

Figure 6. Bland Altman plots of Ktrans from AATHFT versus AATH, ETM, Patlak and Logan. Data points are patient median values of tumor voxels.

4 Discussion

This study compared five models that can be used to estimate K^{trans} for head and neck tumors using DCE-CT. Analysis using AIC showed that AATHFT produces the best fits with the data; this method had the lowest AIC for more than 50%, and the lowest or second lowest AIC for over 95%, of tumor

voxels in all patients. All other models showed significant bias in their estimates of K^{trans} relative to AATHFT. The Patlak model revealed the largest bias, invalidating it for use in tumor DCE-CT.

Although AATHFT showed the best results, the inclusion of mean transit time in the AATH model could theoretically provide a better representation of the contrast passage through the capillaries. However, as shown by Jeukens and Kershaw (Jeukens *et al* 2006, Kershaw and Cheng 2010), the mean transit time and leakage both result in a widening of the first bolus pass. Separation of the effects of mean transit time and leakage is problematic in tumors and requires high frequency information on the first bolus pass. Failure to separate the two can result in over-estimation of T_i and negative T_d values. This issue was shown in the parameter map of T_i (figure 5) and extends to the permeability parameters (K^{trans}, K_{ep}, V_d). Overestimation of T_i in tumors is often reported in literature (Sahani *et al* 2005, Jeukens *et al* 2006, Korporaal *et al* 2012) and results in underestimation of F and K^{trans}, or overestimation of V_i.

Fixing the T_i parameter to a single value leads to a model somewhere between AATH and ETM. In comparison with ETM, AATHFT can better fit a strongly widened first bolus pass while retaining a high correlation and quantitative agreement of K^{trans} estimates with AATH. However this lumps the effects of flow quantity (F) and flow speed (T_i) into the blood volume parameter (V_i) so that information about their separate values is lost.

The ETM representation of intravascular blood flow is rudimentary and does not allow widening of the first bolus pass signal by tissue transit duration, as opposed to AATH. In highly vascularized tissue with a high vascular permeability such as tumor tissue, the simple representation of the capillary system leads to lower estimates of V_i than AATH (Table 3). It is likely that in many cases the first bolus pass signal is attributed to the permeability portion of the model, as was shown in (Sourbron and Buckley 2011).This results in an increase of the K^{trans} estimates and instability in the blood volume parameter (figure 5).

Estimated K^{trans} values from all models, except Patlak, fell within the range generally seen in the literature (Tawfik *et al* 2012, 2011, Bisdas *et al* 2007) (12-18 mL/100g/min). The Patlak model differs from the other investigated models in that it does not include reversible leakage. Because of the low V_d in tumors, TACs that are relatively flat beyond the stable state are common in larynx tumors. Such time curves are interpreted by Patlak to indicate low vascular leakage (figure 3). Low vascular leakage means that most signal is attributed to intravascular contrast instead of interstitial contrast. This results in blood volume estimates up to 32 mL/100g (Table 2), which translates to almost half of the tumor volume being vascular lumen. This suggests that the Patlak model is invalid for tumors. Some researchers suggest (Abramyuk *et al* 2010, Miles *et al* 2012) that for Patlak analysis in tumors, the section of the Patlak plot prior to the stable state should be used. This section of the Patlak plot is however strongly influenced by the first bolus pass and it is unlikely that the Patlak-Blasberg equality (Patlak *et al* 1983), which forms the basis of the Patlak model, holds under such conditions. This makes estimation of K^{trans} using Patlak as proposed in (Miles *et al* 2012) strongly protocol- and patient-dependent.

Spearman's correlations for K^{trans} are strong between all models except Patlak (Table 3). When examining these correlations using Bland-Altman plots (figure 6), large biases but no trends were observed in the plots for the various models except for Patlak, which showed both large bias and trend. Combining these findings shows that the Logan plot, although it has a strong negative bias with a large variance preserves value ordering and has a bias that is largely-value independent. This makes it an acceptable alternative to tracer kinetic model fitting if one is not interested in quantitative values.

4.1 Limitations

This study included a relatively small number of patients. Tumor delineations based on histopathology give a very high certainty that the estimated perfusion parameters are derived from tumorous tissue.

However the process of delineating and registering pathology to DCE-CT is complicated and very time consuming, it is therefore difficult to include a large cohort of patients in such studies.

Although many models exist, we restricted this paper to the most commonly used models for estimating K^{trans}. Numerical studies (Bennink *et al* 2013, Sourbron and Buckley 2012) show that the Distributed Parameter model (DPM) (Sangren and Sheppard 1953), the Tissue Homogeneity model (Johnson and Wilson 1966) and the Distributed Transit-time Model (Bennink *et al* 2013) are largely equivalent to AATH, under the conditions found in larynx tumors (high permeability and large EES). The two-compartment exchange model has been compared with ETM (Sourbron and Buckley 2011) using simulation studies which showed that they yield very different results. Although the two-compartment exchange model is rarely used in clinical studies, it warrants further investigation.

Furthermore the absence of delay corrected versions of the Patlak and Logan linearizations is a shortcoming of this study. However, the AIF and TAC vary little over a period of 3 to 5 seconds after the stable state has ensued therefore such a correction would have little effect and remove the advantage of linearizations over NLR of being faster and simpler to use.

This study was focused almost exclusively on the estimation of K^{trans}. The K^{trans} parameter is the most frequently used parameter for analyzing tumors. In high permeability tissue estimating K^{trans} (or the other permeability parameters K_{ep} and V_d) can be done with more reliability than estimating V_i, T_i and F, regardless of the model. This is because permeability determines a larger portion of the TAC than other parameters and they do not require high frequency temporal information to estimate. More research is required to determine the requirements for quantitative estimation of these other parameters.

4.2 Conclusion

AATHFT was found to be preferable to other examined models for estimating K^{trans} for tumor delineation and characterization in larynx and hypopharynx tumors. AATHFT shows better fits for most tumor voxels, its parameter maps show little spatial noise and its K^{trans} estimates show significant correlation to other models.

The Patlak plot should not be used to estimate K^{trans} in these tumors. The Patlak model assumes irreversible contrast transfer. This assumption is violated by the low distribution volume and high perfusion in larynx tumors.

5 Acknowledgement and funding support

The authors acknowledge Joana Caldas Magalhaes, Stefan Willems and Nina Kooij for their valuable work on the HE tumor delineations and their registration to the DCE-CT data. We would also like to thank Chris Terhaard and Frank Pameijer for their valuable insights in head and neck oncology. This work was supported by a research grant from the Dutch Technology Foundation STW. 'Perspectief' program 'CARISMA', project 'AIRSPACE' (11632). The project 'AIRSPACE' received in-kind funding from Philips Healthcare and the LifeTec Group. The specimens and the imaging was acquired as part of a study supported by the Dutch Cancer Society, Grant No. 2011-5152

6 References

Abramyuk A, Wolf G, Shakirin G, Haberland U, Tokalov S, Koch A, Appold S, Zöphel K and Abolmaali N 2010 Preliminary assessment of dynamic contrast-enhanced CT implementation in pretreatment FDG-PET/CT for outcome prediction in head and neck tumors *Acta Radiologica* **51** 793–799 Online: http://acr.sagepub.com/lookup/doi/10.3109/02841851.2010.491092

Akaike H 1974 A new look at the statistical model identification *Automatic Control, IEEE Transactions on* **19** 716–723 Online: http://ieeexplore.ieee.org/xpls/abs_all.jsp?arnumber=1100705

Bennink E, Riordan A J, Horsch A D, Dankbaar J W, Velthuis B K and Jong H W A M de 2013 A fast nonlinear regression method for estimating permeability in CT perfusion imaging *Journal of Cerebral Blood Flow & Metabolism* **33** 1743–1751 Online: http://www.nature.com/doifinder/10.1038/jcbfm.2013.122

Bisdas S, Konstantinou G N, Lee P S, Thng C H, Wagenblast J, Baghi M and Koh T S 2007 Dynamic contrast-enhanced CT of head and neck tumors: perfusion measurements using a distributed-parameter tracer kinetic model. Initial results and comparison with deconvolution-based analysis *Physics in Medicine and Biology* **52** 6181–6196 Online: http://stacks.iop.org/0031-9155/52/i=20/a=007?key=crossref.a5046d202b49eeb5f6b5450999e41960

Bisdas S, Medov L, Baghi M, Konstantinou G N, Wagenblast J, Thng C H, Vogl T J and Koh T S 2008 A comparison of tumour perfusion assessed by deconvolution-based analysis of dynamic contrast-enhanced CT and MR imaging in patients with squamous cell carcinoma of the upper aerodigestive tract *European Radiology* **18** 843–850 Online: http://link.springer.com/10.1007/s00330-007-0827-3

Caldas-Magalhaes J, Kasperts N, Kooij N, Berg C A T van den, Terhaard C H J, Raaijmakers C P J and Philippens M E P 2012 Validation of Imaging With Pathology in Laryngeal Cancer: Accuracy of the Registration Methodology *International Journal of Radiation Oncology*Biology*Physics* **82** e289–e298 Online: http://linkinghub.elsevier.com/retrieve/pii/S036030161100664X

Van Cann E M, Rijpkema M, Heerschap A, Bilt A van der, Koole R and Stoelinga P J W 2008 Quantitative dynamic contrast-enhanced MRI for the assessment of mandibular invasion by squamous cell carcinoma *Oral Oncology* **44** 1147–1154 Online: http://linkinghub.elsevier.com/retrieve/pii/S1368837508000638

Chawla S, Kim S, Loevner L A, Hwang W-T, Weinstein G, Chalian A, Quon H and Poptani H 2011 Prediction of Disease-Free Survival in Patients with Squamous Cell Carcinomas of the Head and Neck Using Dynamic Contrast-Enhanced MR Imaging *American Journal of Neuroradiology* **32** 778–784 Online: http://www.ajnr.org/cgi/doi/10.3174/ajnr.A2376

Jeukens C R L P N, Berg C A T van den, Donker R, Vulpen M van, Bakker C J G, Leeuwen M S van and Heide U A van der 2006 Feasibility and measurement precision of 3D quantitative blood flow mapping of the prostate using dynamic contrast-enhanced multi-slice CT *Physics in Medicine and Biology* **51** 4329–4343 Online: http://stacks.iop.org/0031-9155/51/i=17/a=013?key=crossref.7a432a25fbc22fdcfb3dd7e4ee5a75c6

Johnson J A and Wilson T A 1966 A model for capillary exchange *American Journal of Physiology–Legacy Content* **210** 1299–1303

Kambadakone A R and Sahani D V 2009 Body Perfusion CT: Technique, Clinical Applications, and Advances *Radiologic Clinics of North America* **47** 161–178 Online: http://linkinghub.elsevier.com/retrieve/pii/S0033838908002108

Kershaw L E and Cheng H-L M 2010 Temporal resolution and SNR requirements for accurate DCE-MRI data analysis using the AATH model *Magnetic Resonance in Medicine* **64** 1772–1780 Online: http://doi.wiley.com/10.1002/mrm.22573

Kim S, Loevner L A, Quon H, Kilger A, Sherman E, Weinstein G, Chalian A and Poptani H 2010 Prediction of Response to Chemoradiation Therapy in Squamous Cell Carcinomas of the Head and Neck Using Dynamic Contrast-Enhanced MR Imaging *American Journal of Neuroradiology* **31** 262–268 Online: http://www.ajnr.org/cgi/doi/10.3174/ajnr.A1817

Klein S, Staring M, Murphy K, Viergever M A and Pluim J 2010 elastix: A Toolbox for Intensity-Based Medical Image Registration *IEEE Transactions on Medical Imaging* **29** 196–205 Online: http://ieeexplore.ieee.org/lpdocs/epic03/wrapper.htm?arnumber=5338015

Konstas A A, Goldmakher G V, Lee T-Y and Lev M H 2009 Theoretic Basis and Technical Implementations of CT Perfusion in Acute Ischemic Stroke, Part 1: Theoretic Basis *American Journal of Neuroradiology* **30** 662–668 Online: http://www.ajnr.org/cgi/doi/10.3174/ajnr.A1487

Korporaal J G, Berg C A T van den, Groenendaal G, Moman M R, Vulpen M van and Heide U A van der 2010 The use of probability maps to deal with the uncertainties in prostate cancer delineation *Radiotherapy and Oncology* **94** 168–172 Online: http://linkinghub.elsevier.com/retrieve/pii/S0167814009006811

Korporaal J G, Vulpen M van, Berg C A T van den and Heide U A van der 2012 Tracer kinetic model selection for dynamic contrast-enhanced computed tomography imaging of prostate cancer *Investigative Radiology* **47** 41–48

Logan J, Fowler J S, Volkow N D, Wolf A P, Dewey S L, Schlyer D J, MacGregor R R, Hitzemann R, Bendriem B, Gatley S J and others 1990 Graphical analysis of reversible radioligand binding from time-activity measurements applied to [N-11C-methyl]-(-)-cocaine PET studies in human subjects *Journal of Cerebral Blood Flow & Metabolism* **10** 740–747

Mendrik A M, Vonken E, Ginneken B van, Jong H W A M de, Riordan A, Seeters T van, Smit E J, Viergever M A and Prokop M 2011 TIPS bilateral noise reduction in 4D CT perfusion scans produces high-quality cerebral blood flow maps *Physics in Medicine and Biology* **56** 3857–3872 Online: http://stacks.iop.org/0031-9155/56/i=13/a=008?key=crossref.a7e3729b03423e270f49fce5aa3966e4

Miles K A, Lee T-Y, Goh V, Klotz E, Cuenod C, Bisdas S, Groves A M, Hayball M P, Alonzi R and Brunner T 2012 Current status and guidelines for the assessment of tumour vascular support with dynamic contrast-enhanced computed tomography *European Radiology* **22** 1430–1441 Online: http://link.springer.com/10.1007/s00330-012-2379-4

Newbold K, Castellano I, Charles-Edwards E, Mears D, Sohaib A, Leach M, Rhys-Evans P, Clarke P, Fisher C, Harrington K and Nutting C 2009 An Exploratory Study Into the Role of Dynamic Contrast-Enhanced Magnetic Resonance Imaging or Perfusion Computed Tomography for Detection of Intratumoral Hypoxia in Head-and-Neck Cancer *International Journal of Radiation Oncology*Biology*Physics* **74** 29–37 Online: http://linkinghub.elsevier.com/retrieve/pii/S0360301608031799

Patlak C S, Blasberg R G, Fenstermacher J D and others 1983 Graphical evaluation of blood-to-brain transfer constants from multiple-time uptake data *Journal of Cerebral Blood Flow & Metabolism* **3** 1–7

Port R E, Bernstein L J, Barboriak D P, Xu L, Roberts T P L and Bruggen N van 2010 Noncompartmental kinetic analysis of DCE-MRI data from malignant tumors: Application to glioblastoma treated with bevacizumab *Magnetic Resonance in Medicine* n/a–n/a Online: http://doi.wiley.com/10.1002/mrm.22399

Sahani D V, Kalva S P, Hamberg L M, Hahn P F, Willett C G, Saini S, Mueller P R and Lee T-Y 2005 Assessing Tumor Perfusion and Treatment Response in Rectal Cancer with Multisection CT: Initial Observations1 *Radiology* **234** 785–792 Online: http://pubs.rsna.org/doi/abs/10.1148/radiol.2343040286

Sangren W and Sheppard C 1953 A mathematical derivation of the exchange of a labeled substance between a liquid flowing in a vessel and an external compartment *Bulletin of Mathematical Biophysics* **15** 387–394

Sanz R, Martí-Bonmatí L, Rodrigo J L and Moratal D 2008 MR pharmacokinetic modeling of the patellar cartilage differentiates normal from pathological conditions *Journal of Magnetic Resonance Imaging* **27** 171–177 Online: http://doi.wiley.com/10.1002/jmri.21233

Sourbron S P and Buckley D L 2011 On the scope and interpretation of the Tofts models for DCE-MRI *Magnetic Resonance in Medicine* **66** 735–745 Online: http://doi.wiley.com/10.1002/mrm.22861

Sourbron S P and Buckley D L 2012 Tracer kinetic modelling in MRI: estimating perfusion and capillary permeability *Physics in Medicine and Biology* **57** R1–R33 Online: http://stacks.iop.org/0031-9155/57/i=2/a=R1?key=crossref.d84ba3ad7b47936a6050433f387d6ebc

St. Lawrence K S and Lee T-Y 1998 An adiabatic approximation to the tissue homogeneity model for water exchange in the brain: I. Theoretical derivation *Journal of Cerebral Blood Flow & Metabolism* **18** 1365–1377

Tawfik A M, Nour-Eldin N-E A, Naguib N N, Razek A A, Denewer A T, Bisdas S and Vogl T J 2012 CT perfusion measurements of head and neck carcinoma from single section with largest tumor dimensions or average of multiple sections: Agreement between the two methods and effect on intra- and inter-observer agreement *European Journal of Radiology* **81** 2692–2696 Online: http://linkinghub.elsevier.com/retrieve/pii/S0720048X11007881

Tawfik A M, Razek A A A, Elsorogy L G, Soliman N Y, Kerl J M, Mack M G and Vogl T J 2011 Perfusion CT of Head and Neck Cancer: Effect of Arterial Input Selection *American Journal of Roentgenology* **196** 1374–1380 Online: http://www.ajronline.org/doi/abs/10.2214/AJR.10.5343

Tofts P S, Brix G, Buckley D L, Evelhoch J L, Henderson E, Knopp M V, Larsson H B, Lee T-Y, Mayr N A and Parker G J 1999 Estimating kinetic parameters from dynamic contrast-enhanced T 1-weighted MRI of a diffusable tracer: standardized quantities and symbols *Journal of Magnetic Resonance Imaging* **10** 223–232 Online: https://tauruspet.med.yale.edu/staff/edm42/IUPUI-website/emorris.tar/emorris/emorris/TracerKineticsCourse2006/Papers/diffusible%20tracers%20and%20MR/kinetic%20params%20from%20CE%20t1-wtd%20MR%20-%20Tofts%20JMRI%201999.pdf

Yang C, Stadler W M, Karczmar G S, Milosevic M, Yeung I and Haider M A 2010 Comparison of quantitative parameters in cervix cancer measured by dynamic contrast-enhanced MRI and CT *Magnetic Resonance in Medicine* **63** 1601–1609 Online: http://doi.wiley.com/10.1002/mrm.22371